High-spin states of ^{95}Tc: towards a systematic investigation of $\nu d_{5/2} \rightarrow \nu g_{7/2}$ excitations along $N = 52$ isotones*

K. K. Zheng (郑宽宽)[1,2] B. S. Cai (蔡博帅)[3] B. Ding (丁兵)[1,2†] M. L. Liu (柳敏良)[1,2‡] Y. H. Qiang (强赟华)[1,2§]
C. X. Yuan (袁岑溪)[3] G. S. Li (李广顺)[1,2] J. G. Wang (王建国)[1,2] S. Guo (郭松)[1,2] C. M. Petrache[1,4]
Y. D. Fang (方永得)[1,2] M. Y. Liu (刘梦瑶)[1,2] Z. Liu (刘忠)[1,2] W. Q. Zhang (张文强)[1,2] F. F. Zeng (曾凡斐)[1,2]
H. Huang (黄浩)[1,2] Q. B. Zeng (曾全波)[1,2] H. Y. Lu (卢洪洋)[1,2] M. Kumar Raju[1,2,5] S. C. Wang (王思成)[1,2]
M. H. Huang (黄明辉)[1,2] Y. Zheng (郑云)[6] S. Y. Wang (王守宇)[7] C. Liu (刘晨)[7] X. C. Han (韩星池)[7]
X. Xiao (肖骁)[7] L. Mu (穆琳)[7] W. Z. Xu (许文政)[7] H. F. Bai (白洪斐)[7] Y. J. Li (李英健)[7] X. D. Wang (王旭东)[7]
L. Zhu (祝霖)[7] H. L. Wang (王华磊)[8] T. X. Li (李天晓)[6] A. Rohilla[7] C. Y. Niu (牛晨阳)[9] X. X. Xu (徐新星)[1,2]
Y. H. Zhang (张玉虎)[1,2] X. H. Zhou (周小红)[1,2]

[1]Key Laboratory of High Precision Nuclear Spectroscopy and Center for Nuclear Matter Science, Institute of Modern Physics, Chinese Academy of Sciences, Lanzhou 730000, China
[2]School of Nuclear Science and Technology, University of Chinese Academy of Sciences, Beijing 100049, China
[3]Sino-French Institute of Nuclear Engineering and Technology, Sun Yat-Sen University, Zhuhai 519082, China
[4]Université Paris-Saclay, CNRS/IN2P3, IJCLab, Orsay 91405, France
[5]Department of Physics, GITAM School of Science, GITAM University, Visakhapatnam 530045, India
[6]China Institute of Atomic Energy, Beijing 102413, China
[7]Shandong Provincial Key Laboratory of Optical Astronomy and Solar-Terrestrial Environment, Institute of Space Sciences, Shandong University, Weihai 264209, China
[8]School of Physics, Zhengzhou University, Zhengzhou 450001, China
[9]School of Physics and State Key Laboratory of Nuclear Physics and Technology, Peking University, Beijing 100871, China

Abstract: High-spin states in ^{95}Tc were investigated via the ^{87}Rb(^{12}C, $4n$)^{95}Tc reaction at a beam energy of 62 MeV using standard in-beam γ-ray spectroscopic techniques. The previously established level scheme was revised and extended through the identification of 42 new transitions. The experimental results are interpreted using large-scale shell-model calculations. Valence-nucleon excitations outside the ^{88}Sr core dominate the excited states up to $J = 33/2$, corresponding to the maximum angular momentum possible within this restricted space. Of particular interest are the systematics of $\nu d_{5/2} \rightarrow \nu g_{7/2}$ excitations across the $N = 56$ subshell. These systematics show that proton excitations across the $Z = 38$ subshell, coupled with neutrons in the $d_{5/2}$ and $g_{7/2}$ orbitals, are necessary for higher-spin states.

Keywords: high-spin states, γ-ray spectroscopy, shell model, N=52 isotones

DOI: 10.1088/1674-1137/ae9ea9 **CSTR:** 32044.14.ChinesePhysicsC.51014001

I. INTRODUCTION

High-spin states in atomic nuclei are generally generated through two distinct mechanisms: the collective mode, associated with the rotation of a deformed nuclear shape, and the non-collective (single-particle) mode, in which angular momentum is generated by the successive alignment of valence nucleons in specific orbitals [1−3]. Although high-j orbitals play a particularly important role in the non-collective mode, medium- and low-j orbitals also contribute significantly to the generation of angular momentum. Nuclei in the $A \approx 90$ mass region, located near the ^{88}Sr ($Z = 38, N = 50$) core, are well known to exhibit predominantly single-particle excitations at low and

Received 21 June 2026; Accepted 25 August 2026; Accepted manuscript online 26 August 2026

* Supported by the National Key R&D Program of China (2024YFE0110400), the Major Science and Technology Projects in Gansu Province (24GD13GA005), the National Natural Science Foundation of China (U2032211, 12575128, 12075287, U2032144, 12205341, U2032135), the Strategic Priority Research Program of the Chinese Academy of Sciences (XDB34010000), and the Special Research Assistant Project of the Chinese Academy of Sciences

† E-mail: dbing@impcas.ac.cn
‡ E-mail: liuml@impcas.ac.cn
§ E-mail: yhqiang@impcas.ac.cn

©2027 Chinese Physical Society and the Institute of High Energy Physics of the Chinese Academy of Sciences and the Institute of Modern Physics of the Chinese Academy of Sciences and IOP Publishing Ltd. All rights, including for text and data mining, AI training, and similar technologies, are reserved.

medium spins [4−14]. The low-lying states in nuclei with $Z > 38$ and $N > 50$ can be interpreted by coupling protons in the $\pi(p_{1/2}, g_{9/2})$ orbitals above the $Z = 38$ shell to neutrons in the $\nu(d_{5/2}, s_{1/2})$ orbitals above the $N = 50$ shell, with ^{88}Sr treated as an inert core. For states at high energy, three competing excitation mechanisms are involved: proton promotion across the $Z = 38$ subshell, neutron excitations across the $N = 50$ closed shell, and neutron excitations through the $N = 56$ subshell ($d_{5/2} \rightarrow g_{7/2}$ excitation). Among these mechanisms, proton excitations across the $Z = 38$ subshell are energetically favored because of the relatively small $Z = 38$ subshell gap [15]. Breaking the $N = 50$ core through neutron $g^{-1}_{9/2}$ excitations has been suggested as a mechanism for generating higher angular momentum in several $N = 52$ isotones, such as ^{94}Mo [7] and ^{96}Ru [5]. The excitation energy required to break the $N = 50$ core increases with proton number, as reported in Refs. [16, 17], whereas the energy of the $\nu g_{7/2}$ orbital decreases. As more protons occupy the $\pi g_{9/2}$ orbital, the $\nu g_{7/2}$ orbital is lowered because of the enhanced proton-neutron attraction resulting from the large wave-function overlap between these spin-orbit partners (see Ref. [9] and references therein).

In ^{95}Tc, breaking of the $N = 50$ core was previously incorporated into shell-model calculations to describe high-spin states [6]. However, large discrepancies remain between theoretical and experimental level energies; these discrepancies were attributed to either the effective interactions or the limited model space used. Recent investigations indicate that neutron $d_{5/2} \rightarrow g_{7/2}$ excitation is energetically more favorable than $N = 50$ core breaking in the $N = 52$ isotones [7−9]. Nevertheless, the $d_{5/2} \rightarrow g_{7/2}$ excitation has not been included in calculations for ^{95}Tc, and the lack of experimental data in the corresponding energy region has further hindered understanding of the dominant excitation mechanisms.

The purpose of the present study is to probe these structural features in ^{95}Tc and to complete the systematics of $d_{5/2} \rightarrow g_{7/2}$ excitations along the $N = 52$ isotones, thereby contributing to a comprehensive understanding of nuclear structure in the $A \sim 90$ region. Prior to this work, low-spin states in ^{95}Tc were observed from electron capture (EC) and isomeric decay [18, 19], as well as from transfer reaction experiments [20]. Previous high-spin work on ^{95}Tc was reported by Ghugre et al. [6], who populated the nucleus through the (HI, α2n) side channel as a by-product of the (HI, xn) and (HI, pxn) reactions using the Early Implementation Gammasphere. Here, we report the experimental results for the high-spin level structure of ^{95}Tc obtained via in-beam γ-ray spectroscopy following a heavy-ion fusion-evaporation reaction.

II. EXPERIMENT

High-spin states in ^{95}Tc were populated via the ^{87}Rb(^{12}C, 4n)^{95}Tc fusion-evaporation reaction using a 62-MeV ^{12}C beam provided by the Sector Focusing Cyclotron at the Heavy Ion Research Facility in Lanzhou (HIRFL) [21]. The target consisted of an 18 μg/cm^2 C foil facing the beam, followed by an ^{87}RbCl foil with a thickness of 4.2 mg/cm^2 and a natural Pb foil with a thickness of 8.7 mg/cm^2. The Pb foil served as the stopper for the reaction residues, and the C foil served as the covering layer for the hygroscopic ^{87}RbCl foil. The emitted γ rays were detected using a multi-detector array [22], which consisted of five Clover detectors of the EXOGAM type [23] grouped into a ring at 90° and fourteen high-purity germanium (HPGe) detectors with a relative efficiency of 70% grouped into four rings at ±52° and ±26° relative to the beam axis. Specifically, four HPGe detectors were placed at each of 52° and 26°, and three were placed at each of 128° and 154°. All detectors were equipped with BGO anti-Compton shields. A total of 1.0×10^9 γ-γ-γ coincidence events were recorded and sorted into a three-dimensional histogram (cube) for subsequent off-line analysis. In addition, 7×10^9 γ-γ coincidence events were recorded. In the experiment, the energy and efficiency calibrations were performed using ^{60}Co, ^{133}Ba, and ^{152}Eu standard sources, and the typical energy resolution was about 2.0−2.5 keV at full width at half-maximum (FWHM) for the 1332.5-keV γ ray of ^{60}Co.

To obtain angular distribution information for the emitted γ rays, γ-ray angular distribution asymmetry ratios from oriented nuclei (ADO), $R_{\rm ADO}(\gamma) = I_\gamma(\pm26°)/I_\gamma(90°)$, were extracted. Two asymmetric matrices were constructed using the γ rays detected at all angles against those observed at ±26° and 90°, respectively. By setting gates on the axis with all detectors, the γ-ray intensities I_γ were extracted from the coincidence spectra regardless of the multipole character of the gating transition. Typical $R_{\rm ADO}(\gamma)$ values were ≈ 1.4 for stretched-quadrupole transitions (or unstretched dipole transitions) and ≈ 0.8 for stretched-dipole transitions, as deduced from known transitions in nuclei produced in the present reaction.

The ADO ratio is mainly sensitive to the transition multipolarity, *i.e.*, the dipole or quadrupole character. However, it does not provide direct information on the electric or magnetic nature of a transition. Therefore, stretched $M1/E2$ mixed transitions and E1 transitions may not be unambiguously distinguished by ADO ratios alone. Consequently, parity assignments derived solely from ADO ratios, in the absence of complementary information such as linear-polarization measurements, must be regarded as tentative. A linear-polarization analysis using the present setup was not feasible because of limited statistics in the coincidence polarization matrices. Accordingly, when the ADO ratios alone are insufficient to determine the parity unambiguously, the parity assignments of the newly observed levels are given in parentheses throughout this work.

III. EXPERIMENTAL RESULTS

Compared with the previous work of Ref. [6], 42 new γ rays and 21 new levels have been incorporated into the level scheme of ^{95}Tc, as shown in Fig. 1. The newly identified levels (transitions) and spin-parity assignments are indicated in red, and the revised spin-parity assignments are indicated in green. Representative γ-ray coincidence spectra are presented in Fig. 2. $R_{\rm ADO}$ ratios of selected transitions in ^{95}Tc are plotted as a function of γ-ray energy in Fig. 3. The measured spectroscopic data, including γ-ray energies, relative intensities, $R_{\rm ADO}$ ratios, multipolarities, and assigned level spin-parities, are summarized in Table 1. It should be noted that the relative intensities of the weak γ rays listed in Table 1 were extracted from the two-dimensional coincidence matrix, which provides higher statistics. In contrast, the coincidence spectra shown in Fig. 2 were generated from the three-dimensional coincidence cube with double gates to suppress contaminant transitions. Consequently, the apparent peak heights of some weak transitions in Fig. 2 may not directly reflect their relative intensities. These spectra are used mainly to establish coincidence relationships, whereas the relative intensities listed in Table 1 were obtained from the two-dimensional coincidence matrix. Extensions and modifications of the level scheme are presented and discussed below.

For the positive-parity states, the present level scheme is consistent with the work of Ref. [6] up to the 5600-keV level, whereas the 660-keV γ ray feeding the 2184-keV level reported in Ref. [6] cannot be confirmed. This γ ray can be traced back to the work of Sarantites [24], which reported a cascade of three strong γ rays with energies of 663,634, and 592 keV feeding the $11/2^+$ state. Later, the 663-keV transition was found to decay from the 2213-keV state to the 1550-keV state, corresponding to a $17/2^- \rightarrow 15/2^+$ transition [25–27], as shown in the present level scheme. It seems unlikely that an intense 660-keV transition should be placed above the $19/2^+$ state with a sudden termination of the γ-ray flux [6].

Based on the measured $R_{\rm ADO}$ value, we assigned E2 multipolarity to the 1682-keV transition. This assignment differs from the tentative M1 assignment in Ref. [6] but agrees with the angular-distribution results in Ref. [24], leading to the $33/2^+$ assignment for the 5600-keV level. Above this state, several γ rays with energies larger than 2 MeV are observed, as shown in the top right of the level scheme and in Fig. 2(a).

The negative-parity states have been extended to an excitation energy of ~9.1 MeV based on the identification of new transitions, as shown in Fig. 2(c). In addition, a sequence consisting of 656-, 582-, and 1134-keV γ rays is firmly established above the $25/2^-$ state at 4127 keV through the observation of linking transitions connecting the negative- and positive-parity states. The $R_{\rm ADO}$ value for the 306-keV γ ray depopulating the $25/2^-$ state is 1.35, consistent with an assignment of either a $\Delta I = 0$ or $\Delta I = 2$ transition, corresponding to a $(25/2^-)$ or $(29/2^-)$ assignment for the 4127-keV level. The latter can be ruled out because it would require an $M2$ multipolarity for the 611-keV transition, which could not compete with the presumed 306-keV $E2$ transition.

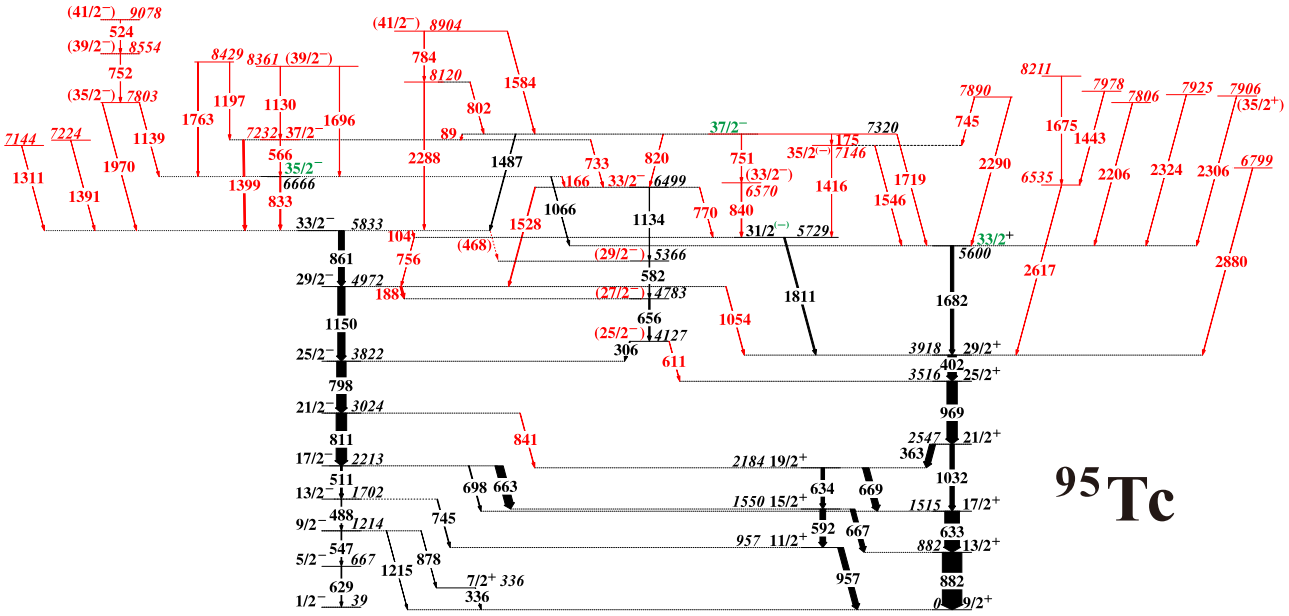


Fig. 1. (color online) Level scheme for ^{95}Tc. Transitions newly observed in the present work are marked in red; spin-parity assignments that differ from those in Ref. [6] are marked in green. Transition energies are given in keV, and the γ-ray intensities are indicated by the arrow widths. Spin-parity values in parentheses are tentative.

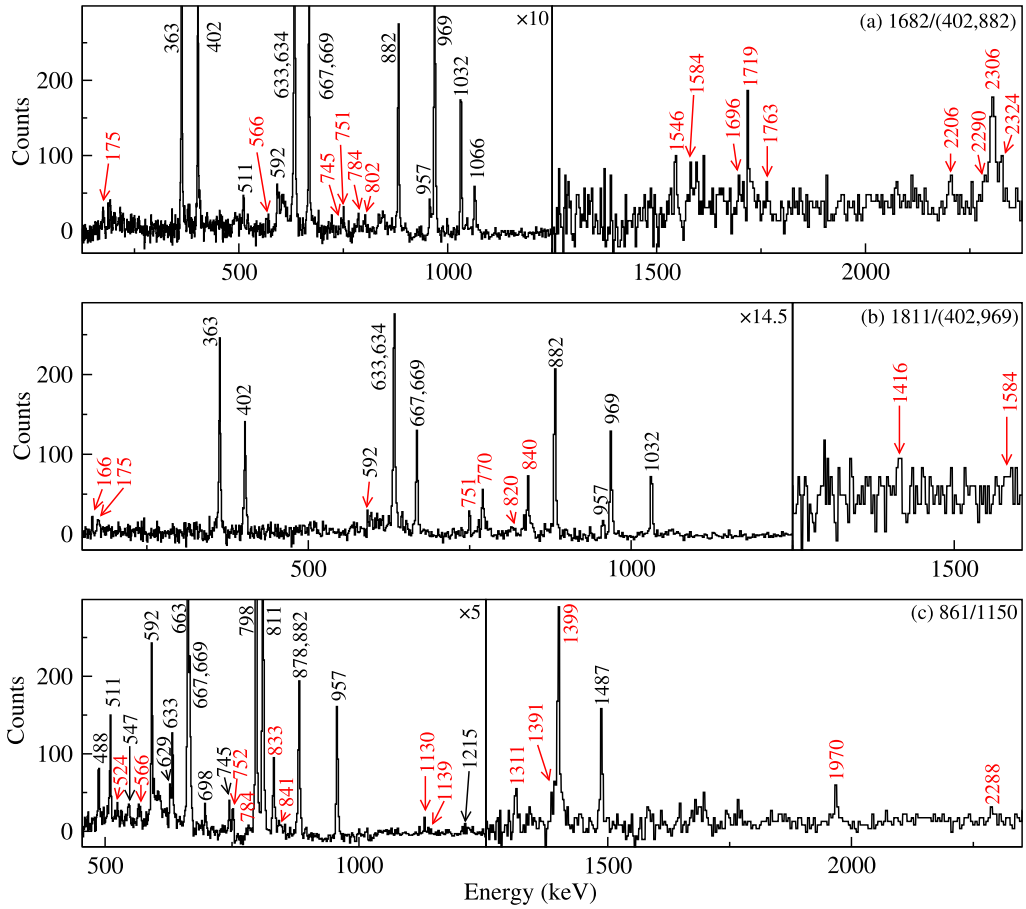


Fig. 2. (color online) Typical double-gated coincidence spectra obtained from the three-dimensional coincidence cube are shown. The spectra in panels (a) and (b) were obtained by summing spectra gated on the transition before the slash and on the transition(s) in parentheses. The newly observed transitions are marked in red.

IV. DISCUSSION

Spherical shell-model calculations were performed to interpret the level structures of the $N = 52$ isotones from ^{90}Sr to ^{97}Rh [4–8, 10, 16, 28]. For ^{95}Tc, the low-lying states up to spin $29/2$ were reasonably described using a model space of $\pi(p_{1/2}, g_{9/2})$ and $\nu(d_{5/2}, s_{1/2})$ with an inert ^{88}Sr core [6]. However, significant discrepancies between predictions and observations were found for the high-spin states because of the limited model space. These discrepancies remained unresolved, even when $N = 50$ core breaking was included in the calculation [6].

Recent studies of the neighboring nucleus ^{93}Nb indicated that breaking of the $N = 50$ core occurs only for states above the $41/2^-$ state at an excitation energy of ~9.1 MeV. In contrast, neutron $d_{5/2} \rightarrow g_{7/2}$ excitations were found to occur at relatively low excitation energies for both positive- and negative-parity states [8]. Similar systematics were observed in other $N = 52$ isotones, such as ^{92}Zr [9] and ^{94}Mo [7]. Indeed, the energy required for the neutron $d_{5/2} \rightarrow g_{7/2}$ excitation was identified to be around 1.6 MeV [7, 9], which is notably close to the energy of the 1682-keV transition feeding the $29/2^+$ state in ^{95}Tc. These systematic features emphasize the need to include such excitations explicitly in the calculations.

In the present work, new transitions have been identified, particularly above the $29/2^{\pm}$ states. To interpret these states, shell-model calculations were performed using the kshell code [29] within an enlarged model space that includes both the neutron $d_{5/2} \rightarrow g_{7/2}$ excitation and neutron $N = 50$ core breaking. The model space includes four proton orbitals $(f_{5/2}, p_{3/2}, p_{1/2}, g_{9/2})$ and seven neutron orbitals $(f_{5/2}, p_{3/2}, p_{1/2}, g_{9/2}, d_{5/2}, g_{7/2}, s_{1/2})$. The Hamiltonian within the f_5pg_9 shell employs the JUN45 interaction [30], whereas the remaining matrix elements are derived from the V_{MU} interaction. Owing to computational limitations, at most one neutron is allowed to be excited from the f_5pg_9 shell to the $g_{7/2}$, $d_{5/2}$, or $s_{1/2}$ orbitals [31]. The largest M-scheme dimension under this $1p-1h$ truncation is approximately 6.7×10^7.

Before comparing the experimental level scheme with the shell-model calculations, we comment on the robustness of the spin-parity assignments. The ADO analysis described in Section III provides reliable discrimination

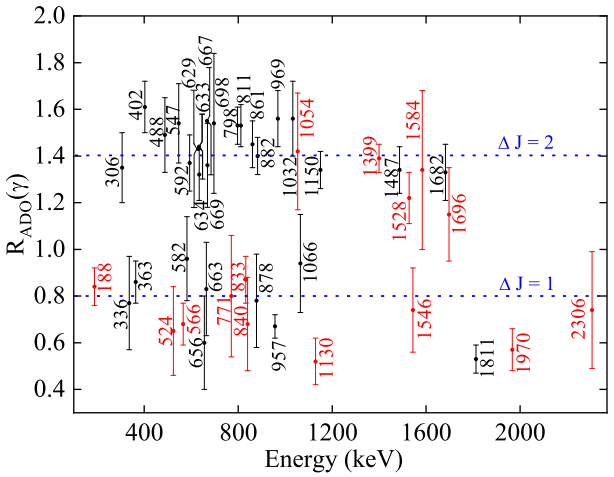


Fig. 3. (color online) The R_{ADO} values for selected transitions in ^{95}Tc as a function of γ-ray energy. Newly observed and previously reported transitions are indicated in red and black, respectively. The quoted uncertainties include contributions from background subtraction, fitting, and efficiency correction.

among stretched dipole ($\Delta J = 1$), stretched quadrupole ($\Delta J = 2$), and $\Delta J = 0$ transitions, but it cannot distinguish $E1$ from $M1/E2$ character on a transition-by-transition basis. Consequently, the parities of several newly proposed levels cannot be firmly established from the present data alone. These include the parities of the $(25/2^-)$ level at 4127 keV, the $(31/2^-)$ level at 5729 keV and the higher-lying level at 6570 keV that feeds it, the $(35/2^-)$ level at 7803 keV and the levels at 8554 and 9078 keV, the $(35/2^+)$ level at 7906 keV, and the $(39/2^-)$ level at 8361 keV. These assignments should therefore be regarded as tentative.

A comparison between the experimental excitation energies and the shell-model predictions for the levels in ^{95}Tc is presented in Fig. 4. For a given spin and parity, the shell-model calculations often predict several states close in energy. Throughout this work, the experimental levels are matched to the calculated states on the basis of the ordering of excitation energies and the yrast-population criterion. When only one experimental level is known for a given J^π, it is associated with the lowest calculated state. When two or more experimental levels are observed, they are matched to the calculated states in increasing order of excitation energy. The calculated transition probabilities for the high-lying states are subject to larger uncertainties because of the model-space truncation; therefore, the correspondence is established primarily on the basis of excitation energies and decay patterns rather than $B(M1)$ or $B(E2)$ values. The calculated levels show reasonable agreement with the experimental data, particularly for the low-lying states up to ~4 MeV. Above this energy, the discrepancies increase, especially for the negative-parity states. The dominant wave functions and seniorities of the positive- and negative-parity states are listed in Tables 2 and 3, respectively. Here, the M-scheme many-body wave functions are expanded in an orbit-wise seniority basis and classified by proton seniority ν_p and neutron seniority ν_n, obtained by summing the seniorities over the proton and neutron orbitals, respectively.

For positive-parity states, the $9/2^+$ ground state is dominated by a single proton in the $g_{9/2}$ orbital with seniority $\nu = 1$. This state is followed by a group of seniority-three states based on the configuration of one $g_{9/2}$ proton coupled to a broken neutron pair in the $d_{5/2}$ orbital, *i.e.*, $\nu d^2_{5/2}$, up to the $17/2^+$ state. In particular, the 882-keV energy of the $13/2^+$ state in ^{95}Tc is very close to those of the 2^+ states in the even-even $N = 52$ isotones, *i.e.*, 831, 934, 871, and 833 keV in ^{90}Sr [12−14], ^{92}Zr [9], ^{94}Mo [7], and ^{96}Ru [5], respectively. The predominant configuration of these 2^+ states is $\nu d^2_{5/2}$. The $19/2^+$ and $21/2^+$ states are predicted to involve mainly the $\nu(d_{5/2}g_{7/2})$ component. This indicates that the neutron $d_{5/2} \rightarrow g_{7/2}$ excitation begins at an excitation energy of ~2.2 MeV. Above the three-particle fully aligned $21/2^+$ state, an additional nuc-

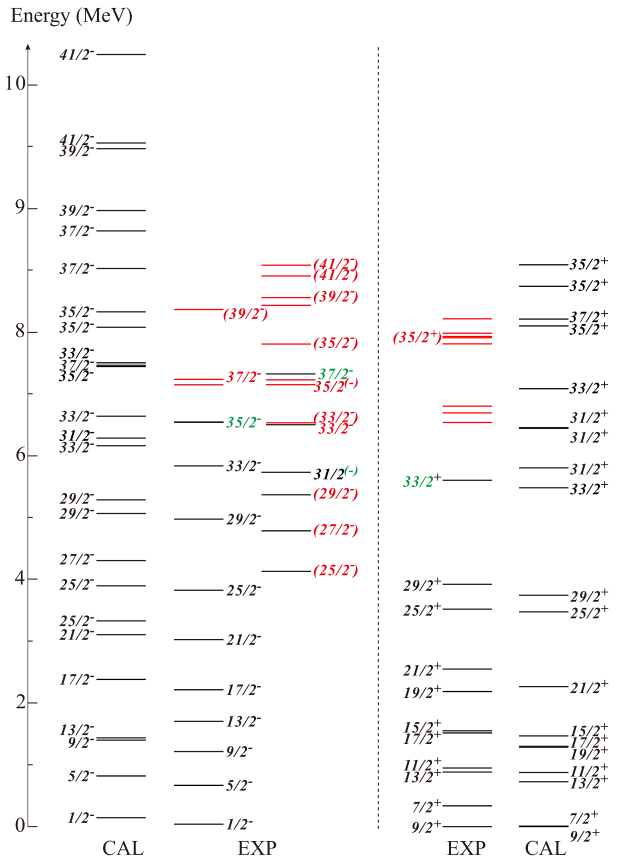


Fig. 4. (color online) Comparison of experimental levels in ^{95}Tc with shell-model predictions. As in Fig. 1, newly observed levels are indicated in red, and levels with revised spin-parity assignments are shown in green. Tentative spin-parity assignments are shown in parentheses.

Table 1. Experimental information, including the γ-ray energies E_γ, relative intensities I_γ, R_{ADO} ratios, multipolarities, initial and final level energies, and spin-parity assignments in ^{95}Tc.

E_γ^a/keV	I_γ^{b*}	$R^*_{\rm ADO}$	Multipolarities^c	$E_i \rightarrow E_f$/keV^d	$J_i^\pi \rightarrow J_f^{\pi e}$
89.1	< 0.4(3)			7319.8 → 7231.6	$37/2^- \rightarrow 37/2^-$
104.4	0.2(1)			5832.7 → 5729.2	$33/2^- \rightarrow 31/2^{(-)}$
165.9	0.5(3)			6665.5 → 6499.3	$35/2^- \rightarrow 33/2^-$
175.2	1.0(5)			7319.8 → 7145.5	$37/2^- \rightarrow 35/2^{(-)}$
188.1	1.8(8)	0.84(8)	(*M*1/*E*2)	4971.6 → 4783.4	$29/2^- \rightarrow (27/2^-)$
305.6	4.4(18)	1.35(15)	(*M*1/*E*2)	4127.4 → 3822.0	$(25/2^-) \rightarrow 25/2^-$
336.0	1.0(4)	0.77(20)	(*M*1/*E*2)	336.0 → 0.0	$7/2^+ \rightarrow 9/2^+$
363.4	30(3)	0.86(9)	(*M*1/*E*2)	2547.2 → 2183.8	$21/2^+ \rightarrow 19/2^+$
402.3	43(4)	1.61(11)	*E*2	3918.4 → 3516.1	$29/2^+ \rightarrow 25/2^+$
468.3	<1.0(9)			5832.7 → 5365.5	$33/2^- \rightarrow (29/2^-)$
487.8	3.4(15)	1.49(16)	*E*2	1702.2 → 1214.4	$13/2^- \rightarrow 9/2^-$
510.7	8(4)	1.22(12)	(*E*2)	2212.9 → 1702.2	$17/2^- \rightarrow 13/2^-$
523.7	1.0(5)	0.65(19)	(*M*1/*E*2)	9078.0 → 8554.3	$(41/2^-) \rightarrow (39/2^-)$
547.0	3.7(19)	1.54(17)	*E*2	1214.4 → 667.4	$9/2^- \rightarrow 5/2^-$
566.1	0.8(7)	0.68(9)	(*M*1/*E*2)	7231.6 → 6665.5	$37/2^- \rightarrow 35/2^-$
582.1	3.3(17)	0.96(18)	(*M*1/*E*2)	5365.5 → 4783.4	$(29/2^-) \rightarrow (27/2^-)$
592.3	30(7)	1.37(12)	*E*2	1549.5 → 957.2	$15/2^+ \rightarrow 11/2^+$
610.8	2.1(15)	1.1(2)	(*E*1)	4127.4 → 3516.1	$(25/2^-) \rightarrow 25/2^+$
628.9	3.7(19)	1.43(25)	*E*2	667.4 → 38.5	$5/2^- \rightarrow 1/2^-$
633.0	75(15)	1.44(14)	*E*2	1515.3 → 882.3	$17/2^+ \rightarrow 13/2^+$
634.4	18(10)	1.32(11)	*E*2	2183.8 → 1549.5	$19/2^+ \rightarrow 15/2^+$
656.0	7(2)	0.6(2)	(*M*1/*E*2)	4783.4 → 4127.4	$(27/2^-) \rightarrow (25/2^-)$
663.4	39(13)	0.82(20)	*E*1	2212.9 → 1549.5	$17/2^- \rightarrow 15/2^+$
667.3	25(9)	1.55(23)	(*M*1/*E*2)	1549.5 → 882.3	$15/2^+ \rightarrow 13/2^+$
668.5	32(12)	1.36(20)	(*M*1/*E*2)	2183.8 → 1515.3	$19/2^+ \rightarrow 17/2^+$
697.5	4(1)	1.54(30)	*E*1	2212.9 → 1515.3	$17/2^- \rightarrow 17/2^+$
732.7	1.3(7)			7231.6 → 6499.3	$37/2^- \rightarrow 33/2^-$
745.0	1.0(7)			7889.9 → 7145.5	$\rightarrow 35/2^{(-)}$
745.2	3.5(11)			1702.2 → 957.2	$13/2^- \rightarrow 11/2^+$
750.6	1.6(7)			7319.8 → 6569.6	$37/2^- \rightarrow (33/2^-)$
751.8	1.4(8)	1.19(27)	(*E*2)	8554.3 → 7802.5	$(39/2^-) \rightarrow (35/2^-)$
755.7	0.6(4)			5729.2 → 4971.6	$31/2^{(-)} \rightarrow 29/2^-$
770.1	1.2(5)	0.80(26)	(*M*1/*E*2)	6499.3 → 5729.2	$33/2^- \rightarrow 31/2^{(-)}$
783.6	0.5(4)			8903.6 → 8120.3	$(41/2^-) \rightarrow$
797.9	48(10)	1.53(8)	*E*2	3822.0 → 3024.1	$25/2^- \rightarrow 21/2^-$
801.5	<0.6(6)			8120.3 → 7319.8	$\rightarrow 37/2^-$
811.2	52(10)	1.53(9)	*E*2	3024.1 → 2212.9	$21/2^- \rightarrow 17/2^-$
819.9	1.3(8)	1.27(35)	(*E*2)	7319.8 → 6499.3	$37/2^- \rightarrow 33/2^-$
832.7	5.6(14)	0.87(10)	(*M*1/*E*2)	6665.5 → 5832.7	$35/2^- \rightarrow 33/2^-$
840.4	3.7(8)	0.68(20)	(*M*1/*E*2)	6569.6 → 5729.2	$(33/2^-) \rightarrow 31/2^{(-)}$
841.2	2.5(13)			3024.1 → 2183.8	$21/2^- \rightarrow 19/2^+$

Table 1-continued from previous page

E_γ^a/keV	I_γ^{b*}	$R^*_{\rm ADO}$	Multipolarities[c]	$E_i \rightarrow E_f$/keV[d]	$J_i^\pi \rightarrow J_f^{\pi e}$
861.1	30(7)	1.45(10)	$E2$	5832.7 → 4971.6	$33/2^- \rightarrow 29/2^-$
878.1	1.0(5)	0.78(20)	$E1$	1214.4 → 336.0	$9/2^- \rightarrow 7/2^+$
882.3	100	1.40(8)	$E2$	882.3 → 0.0	$13/2^+ \rightarrow 9/2^+$
957.2	30(3)	0.67(5)	($M1/E2$)	957.2 → 0.0	$11/2^+ \rightarrow 9/2^+$
968.9	53(3)	1.56(12)	$E2$	3516.1 → 2547.2	$25/2^+ \rightarrow 21/2^+$
1031.8	22(3)	1.56(16)	$E2$	2547.2 → 1515.3	$21/2^+ \rightarrow 17/2^+$
1053.7	2.5(13)	1.42(25)	$E1$	4971.6 → 3918.4	$29/2^- \rightarrow 29/2^+$
1065.6	1.4(6)	0.94(21)	$E1$	6665.5 → 5600.4	$35/2^- \rightarrow 33/2^+$
1129.6	1.7(8)	0.52(10)	($M1/E2$)	8361.3 → 7231.6	$(39/2^-) \rightarrow 37/2^-$
1133.6	1.6(9)			6499.3 → 5365.5	$33/2^- \rightarrow (29/2^-)$
1138.8	0.3(1)			7802.5 → 6665.5	$(35/2^-) \rightarrow 35/2^-$
1149.6	37(11)	1.34(8)	$E2$	4971.6 → 3822.0	$29/2^- \rightarrow 25/2^-$
1196.6	0.4(3)			8428.5 → 7231.6	$\rightarrow 37/2^-$
1214.9	0.2(1)			1214.4 → 0.0	$9/2^- \rightarrow 9/2^+$
1311.2	1.0(5)			7143.9 → 5832.7	$\rightarrow 33/2^-$
1391.1	1.0(5)			7223.8 → 5832.7	$\rightarrow 33/2^-$
1398.8	8.4(24)	1.39(6)	$E2$	7231.6 → 5832.7	$37/2^- \rightarrow 33/2^-$
1415.6	0.5(4)			7145.5 → 5729.2	$35/2^{(-)} \rightarrow 31/2^{(-)}$
1443.0	0.5(4)			7978.3 → 6535.3	
1486.7	3.2(13)	1.34(10)	$E2$	7319.8 → 5832.7	$37/2^- \rightarrow 33/2^-$
1527.8	3.5(15)	1.22(11)	$E2$	6499.3 → 4971.6	$33/2^- \rightarrow 29/2^-$
1545.7	1.0(7)	0.74(18)	($E1$)	7145.5 → 5600.4	$35/2^{(-)} \rightarrow 33/2^+$
1583.7	1.6(8)	1.34(34)	$E2$	8903.6 → 7319.8	$(41/2^-) \rightarrow 37/2^-$
1675.3	0.5(4)			8210.6 → 6535.3	
1682.0	17(4)	1.33(12)	$E2$	5600.4 → 3918.4	$33/2^+ \rightarrow 29/2^+$
1695.9	3.4(12)	1.15(20)	($E2$)	8361.3 → 6665.5	$(39/2^-) \rightarrow 35/2^-$
1719.3	0.6(4)			7319.8 → 5600.4	$37/2^- \rightarrow 33/2^+$
1763.3	0.5(3)			8428.5 → 6665.5	$\rightarrow 35/2^-$
1811.0	8(3)	0.53(6)	($E1$)	5729.2 → 3918.4	$31/2^{(-)} \rightarrow 29/2^+$
1969.5	1.6(6)	0.57(9)	($M1/E2$)	7802.5 → 5832.7	$(35/2^-) \rightarrow 33/2^-$
2205.7	0.5(3)			7806.1 → 5600.4	$\rightarrow 33/2^+$
2287.6	0.6(2)			8120.3 → 5832.7	$\rightarrow 33/2^-$
2289.5	0.4(3)			7889.9 → 5600.4	$\rightarrow 33/2^+$
2305.6	1.0(4)	0.74(25)	($M1/E2$)	7906.0 → 5600.4	$(35/2^+) \rightarrow 33/2^+$
2324.4	0.5(3)			7924.8 → 5600.4	$\rightarrow 33/2^+$
2616.9	1.4(7)			6535.3 → 3918.4	$\rightarrow 29/2^+$
2880.2	2.0(7)			6798.6 → 3918.4	$\rightarrow 29/2^+$

[a]The error on the transition energies is 0.3 keV for transitions below 1000 keV and intensities larger than 5, 0.7 keV for transitions above 1000 keV and intensities larger than 5, and 1.2 keV for transitions above 1500 keV and/or weaker than 5.

[b]Relative γ-ray intensities corrected for efficiency are normalized to the intensity of the 882.3-keV, $13/2^+ \rightarrow 9/2^+$ transition.

[c]The notation $M1/E2$ denotes a mixed $M1+E2$ transition.

[d]Excitation energies of initial (E_i) and final (E_f) states.

[e]Proposed spin-parity assignments for the initial J_i^π and final J_f^π levels.

[*]For γ-ray energies above ~1.5 MeV, the efficiency calibration is obtained by extrapolation, and the quoted intensities and R_{ADO} ratios may carry additional systematic uncertainties.

Table 2. Main partitions of the wave functions for positive-parity states in ^{95}Tc. J_p and J_n denote the angular momenta formed by the valence protons and neutrons, respectively, whereas ν_p and ν_n denote the corresponding proton and neutron seniorities. In the calculations, only one neutron is allowed to be excited across the $N=50$ shell to the $d_{5/2}$, $g_{7/2}$, and $s_{1/2}$ orbitals.

J^π	Proton	Neutron	Partitions
	$(0f_{5/2},1p_{3/2},1p_{1/2},0g_{9/2})^{\nu_p}_{J_p}$	$(0g_{7/2},1d_{5/2})^{\nu_n}_{J_n}$	
$9/2^+$	$(6,4,2,3)^1_{9/2^+}$	$(0,2)^0_{0^+}$	31.88
	$(6,4,2,3)^3_{7/2^+}$	$(0,2)^2_{2^+}$	7.74
$11/2^+$	$(6,4,2,3)^1_{9/2^+}$	$(0,2)^2_{2^+}$	28.78
	$(6,4,2,3)^3_{11/2^+}$	$(0,2)^0_{0^+}$	10.68
$13/2^+$	$(6,4,2,3)^1_{9/2^+}$	$(0,2)^2_{2^+}$	27.06
	$(6,4,2,3)^3_{13/2^+}$	$(0,2)^0_{0^+}$	12.61
$15/2^+$	$(6,4,2,3)^1_{9/2^+}$	$(0,2)^2_{4^+}$	36.07
	$(6,4,2,3)^3_{7/2^+}$	$(0,2)^2_{4^+}$	12.30
$17/2^+$	$(6,4,2,3)^1_{9/2^+}$	$(0,2)^2_{4^+}$	41.98
	$(6,4,2,3)^3_{13/2^+}$	$(0,2)^2_{2^+}$	7.47
$19/2^+$	$(6,4,2,3)^3_{7/2^+}$	$(1,1)^2_{6^+}$	21.02
	$(6,4,2,3)^1_{9/2^+}$	$(1,1)^2_{6^+}$	14.93
$21/2^+$	$(6,4,2,3)^1_{9/2^+}$	$(1,1)^2_{6^+}$	23.54
	$(6,4,0,5)^1_{9/2^+}$	$(1,1)^2_{6^+}$	8.22
$25/2^+$	$(6,4,2,3)^3_{17/2^+}$	$(0,2)^2_{4^+}$	38.97
	$(6,4,2,3)^3_{21/2^+}$	$(0,2)^2_{2^+}$	21.51
$29/2^+$	$(6,4,2,3)^3_{21/2^+}$	$(0,2)^2_{4^+}$	71.01
	$(6,4,0,5)^3_{21/2^+}$	$(0,2)^2_{4^+}$	3.75
$33/2^+$	$(6,4,2,3)^3_{21/2^+}$	$(1,1)^2_{6^+}$	59.05
	$(6,4,0,5)^3_{21/2^+}$	$(1,1)^2_{6^+}$	8.48
$35/2^+$	$(6,4,0,5)^5_{25/2^+}$	$(1,1)^2_{6^+}$	35.36
	$(6,3,1,5)^7_{23/2^+}$	$(1,1)^2_{6^+}$	15.21
$37/2^+$	$(6,4,0,5)^5_{25/2^+}$	$(1,1)^2_{6^+}$	38.52
	$(6,3,1,5)^7_{25/2^+}$	$(1,1)^2_{6^+}$	17.72
$39/2^+$	$(6,3,1,5)^7_{27/2^+}$	$(1,1)^2_{6^+}$	42.10
	$(6,3,1,5)^7_{29/2^+}$	$(1,1)^2_{6^+}$	10.16
$41/2^{+*}$	$(5,4,1,5)^7_{29/2^+}$	$(1,1)^2_{6^+}$	24.78
	$(5,4,1,5)^7_{29/2^+}$	$(1,1)^2_{6^+}$	21.74

* The proton couplings differ between the two main configurations: $(f^5_{5/2}p^1_{1/2})_{3^+}\otimes(g^5_{9/2})_{25/2^+}$ (upper) and $(f^5_{5/2}p^1_{1/2})_{2^+}\otimes(g^5_{9/2})_{25/2^+}$ (lower).

leon pair must be broken to generate further excitations. The higher-spin states therefore have seniority-5 configurations. Shell-model calculations predict that the breaking of a $\pi g_{9/2}$ pair is responsible for the states up to the $33/2^+$ state. Above this state, proton excitations from the $f_{5/2}$ or $p_{3/2}$ orbitals across the $Z=38$ shell to the $g_{9/2}$ orbital become important. Among the transitions depopulating the levels around 7800−7900 keV, the 2306-keV γ ray is the strongest, suggesting that the 7906-keV level depopulated by this transition is more likely to be the yrast $(35/2^+)$ state, consistent with the yrast-population criterion discussed above.

Table 3. Similar to Table 2, but for negative-parity states.

J^π	Proton	Neutron	Partitions
	$(0f_{5/2},1p_{3/2},1p_{1/2},0g_{9/2})^{\nu_p}_{J_p}$	$(0g_{7/2},1d_{5/2})^{\nu_n}_{J_n}$	
$1/2^-$	$(6,4,1,4)^1_{1/2^-}$	$(0,2)^0_{0^+}$	34.95
	$(6,4,1,4)^3_{5/2^-}$	$(0,2)^2_{2^+}$	8.75
$5/2^-$	$(6,4,1,4)^3_{5/2^-}$	$(0,2)^0_{0^+}$	23.03
	$(6,4,1,4)^1_{1/2^-}$	$(0,2)^2_{2^+}$	18.01
$9/2^-$	$(6,4,1,4)^5_{9/2^-}$	$(0,2)^0_{0^+}$	17.24
	$(6,4,1,4)^3_{5/2^-}$	$(0,2)^2_{2^+}$	13.94
$13/2^-$	$(6,4,1,4)^1_{1/2^-}$	$(1,1)^2_{6^+}$	20.04
	$(6,4,1,4)^3_{5/2^-}$	$(1,1)^2_{6^+}$	13.68
$17/2^-$	$(6,4,1,4)^3_{17/2^-}$	$(0,2)^0_{0^+}$	30.45
	$(6,4,1,4)^5_{13/2^-}$	$(0,2)^2_{2^+}$	10.26
$21/2^-$	$(6,4,1,4)^3_{17/2^-}$	$(0,2)^2_{2^+}$	23.90
	$(6,4,1,4)^5_{13/2^-}$	$(0,2)^2_{4^+}$	10.89
$25/2^-$	$(6,4,1,4)^5_{13/2^-}$	$(1,1)^2_{6^+}$	21.88
	$(6,4,1,4)^5_{15/2^-}$	$(1,1)^2_{6^+}$	12.84
$29/2^-$	$(6,4,1,4)^5_{21/2^-}$	$(0,2)^2_{4^+}$	26.27
	$(6,4,1,4)^3_{17/2^-}$	$(1,1)^2_{6^+}$	24.20
$31/2^-$	$(6,4,1,4)^5_{25/2^-}$	$(0,2)^2_{4^+}$	47.16
	$(6,4,1,4)^5_{21/2^-}$	$(1,1)^2_{6^+}$	11.03
$33/2^-$	$(6,4,1,4)^5_{25/2^-}$	$(0,2)^2_{4^+}$	77.21
	$(6,3,2,4)^5_{25/2^-}$	$(0,2)^2_{4^+}$	1.59
$35/2^-$	$(6,4,1,4)^5_{25/2^-}$	$(1,1)^2_{6^+}$	56.05
	$(6,3,2,4)^5_{23/2^-}$	$(1,1)^2_{6^+}$	17.70
$37/2^-$	$(6,4,1,4)^5_{25/2^-}$	$(1,1)^2_{6^+}$	70.69
	$(6,3,2,4)^5_{25/2^-}$	$(1,1)^2_{6^+}$	5.25
$39/2^-$	$(5,4,2,4)^5_{27/2^-}$	$(1,1)^2_{6^+}$	43.65
	$(6,3,2,4)^5_{27/2^-}$	$(1,1)^2_{6^+}$	17.94
$41/2^-$	$(5,4,2,4)^5_{29/2^-}$	$(1,1)^2_{6^+}$	69.00
	$(5,4,0,6)^5_{29/2^-}$	$(1,1)^2_{6^+}$	6.30

It should be noted that although the ADO ratios of the 667.3- and 668.5-keV transitions are close to the values expected for $E2$ radiation, both transitions connect states with ΔI=1 and are assigned as mixed $M1/E2$ transitions. According to the shell-model calculations, the 668.5-keV transition involves a change in the dominant neutron occupation from $\nu(g_{7/2}d_{5/2})$ to $\nu(d^2_{5/2})$. The corresponding $g_{7/2} \rightarrow d_{5/2}$ neutron transition has $\Delta l = 2$, making the $M1$ component l-forbidden and strongly hindered. The relative $E2$ contribution can therefore be substantial, resulting in an $E2$-like ADO ratio. In contrast, the states connected by the 667.3-keV transition have similar proton and neutron orbital occupancies but may differ in the angular-momentum coupling of the proton configuration. The transition could thus be regarded as occurring between different proton-coupling multiplets, for which a sizable $E2$ admixture is consistent with the observed ADO ratio.

As shown in Table 3, the dominant proton contribution to nearly all negative-parity states includes a particle occupying the $p_{1/2}$ orbital. The lowest $1/2^-$ state has the pure single-particle configuration $\pi p_{1/2}$. The $5/2^-$, $9/2^-$, and $17/2^-$ states mainly arise from the coupling of $\pi p_{1/2}$ to a broken proton pair in the $g_{9/2}$ orbital, whereas the $13/2^-$ state arises from the coupling of $\pi p_{1/2}$ with two neutrons in the $\nu(d_{5/2}g_{7/2})$ configuration. This indicates that the neutron $d_{5/2} \rightarrow g_{7/2}$ excitation occurs at ~1.7 MeV, lower than that in positive-parity states (~2.2 MeV). For the higher-lying states, the dominant configuration is $\pi(p_{1/2}g_{9/2})^5 \otimes \nu(d_{5/2}/g_{7/2})^2$ with a seniority of 7. The maximum angular momentum of this configuration is $37/2^-$. Therefore, excitation of a proton from the $\pi p_{3/2}$ orbital and subsequently from the $\pi f_{5/2}$ orbital into the $\pi g_{9/2}$ orbital is necessary to form the even higher-spin states with $J = 39/2$ and $J = 41/2$, respectively. In addition, shell-model calculations predict several $43/2$ states dominated by the $N = 50$ core excitation, but they are not observed experimentally.

V. NEUTRON $d_{5/2} \rightarrow g_{7/2}$ EXCITATION IN $N = 52$ ISOTONES

As shown in Table 2, the $29/2^+$ and $33/2^+$ states, while having identical proton configurations, are characterized by relatively pure neutron components: predominantly $\nu d^2_{5/2}$ for the former and $\nu(d_{5/2}g_{7/2})$ for the latter. The 1682-keV transition between them therefore provides an excellent example of the $d_{5/2} \rightarrow g_{7/2}$ excitation.

In the framework of the spin-isospin-dependent central force [32–34], the enhanced $\pi g_{9/2} - \nu g_{7/2}$ monopole interaction lowers the energy of the $\nu g_{7/2}$ orbital, leading to a $\nu(d_{5/2} \rightarrow g_{7/2})$ excitation of ~1.0 MeV in $N = 52$ isotones with $38 < Z < 45$ [9, 35]. Specifically, in ^{92}Zr and ^{93}Nb, the yrast $(12^+) \rightarrow (14^+)$ and $29/2^{(+)} \rightarrow 33/2^{(+)}$ excitations are attributed to the $\nu(d_{5/2} \rightarrow g_{7/2})$ excitations, with corresponding transition energies of 1098 [9] and 1040 keV [35], as shown in Fig. 5. However, the energy required for the $29/2^+ \rightarrow 33/2^+$ excitation in ^{95}Tc is 1682 keV, substantially larger than expected. This value closely matches that of the adjacent even-even core nucleus ^{94}Mo (1609 keV, Fig. 5). These four nuclei can therefore be classified into two groups: ^{95}Tc and ^{94}Mo, which exhibit unexpectedly high excitation energies, and ^{92}Zr and ^{93}Nb, which belong to the other category. The increase in excitation energy may be accounted for by configuration mixing, as discussed below.

We begin with the even-even nucleus ^{92}Zr, which can be readily described as two protons and two neutrons outside the ^{88}Sr core. The aforementioned 12^+ level is the fully aligned four-particle state based on the pure configuration $\pi(g_{9/2})^2_{8^+} \otimes \nu(d_{5/2})^2_{4^+}$. Similarly, the $29/2^+$ state in ^{93}Nb is expected to arise from the pure configuration involving an additional $\pi g_{9/2}$ valence proton. In ^{94}Mo, four protons are available outside the ^{88}Sr core. Two 12^+ states can be generated by coupling $\pi(g^2_{9/2})_{8^+}$ or $\pi(g^4_{9/2})_{8^+}$ to $\nu(d^2_{5/2})_{4^+}$, respectively. Configuration mixing produces repulsion between the two intrinsic states, lowering the lower level and raising the higher level in energy. Furthermore, when only two $g_{9/2}$ protons are aligned, the pairing interaction (pairing scattering) could occur between $\pi(g^2_{9/2})_{0^+}$ and $\pi(p^2_{1/2})_{0^+}$ [36], leading to enhanced level repulsion. As shown in Fig. 5, the level repulsion lowers the 12^+ and $29/2^+$ states, as well as all the states below them, relative to the corresponding states in ^{92}Zr

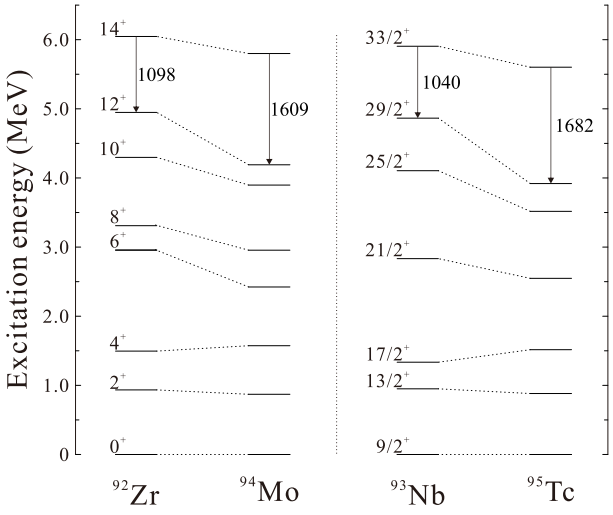


Fig. 5. Comparison of the excitation energies of positive-parity states in $N = 52$ isotones. All states in ^{94}Mo (^{95}Tc) lie systematically lower in energy than these corresponding states in ^{92}Zr (^{93}Nb). The only exceptions are the 4^+ and $17/2^+$ states, which may be attributed to their pure, fully aligned configurations, $\nu(d^2_{5/2})_{4^+}$ and $\pi g_{9/2} \otimes \nu(d^2_{5/2})_{4^+}$, respectively. The data for ^{95}Tc are from this work, whereas those for the other isotopes are from the following Refs.: ^{92}Zr [9], ^{93}Nb [8], and ^{94}Mo [7].

and ^{93}Nb, respectively.

It should be noted that the pairing-scattering mechanism qualitatively explains the systematic lowering of many states in ^{94}Mo and ^{95}Tc compared with ^{92}Zr and ^{93}Nb. However, this simple picture encounters difficulties when examined in detail. The $29/2^+$ state in ^{95}Tc has a remarkably pure dominant configuration (71%, see Table 2), suggesting a relatively pure state that should not be strongly affected by configuration mixing. Nevertheless, the $29/2^+ \rightarrow 33/2^+$ energy gap is exceptionally large (1682 keV), indicating that this state has undergone a substantial downward shift. This inconsistency, together with the observation that the 4^+ and $17/2^+$ states are actually higher in ^{94}Mo and ^{95}Tc, indicates that the simple two-state repulsion picture is incomplete.

VI. SUMMARY

The high-spin levels in ^{95}Tc have been studied using in-beam γ-ray spectroscopy via the ^{87}Rb(^{12}C, $4n$)^{95}Tc fusion-evaporation reaction. The level scheme has been extended by 42 γ transitions, reaching an excitation energy of ~9 MeV. Large-scale shell-model calculations have been performed and reproduce the experimental levels with good accuracy, providing a consistent interpretation of the observed level structure. The low-lying states in ^{95}Tc are described by a proton in the $(p_{1/2}, g_{9/2})$ orbitals coupled to $d_{5/2}$ neutrons, with an inert ^{88}Sr core. With increasing excitation energy, $d_{5/2} \rightarrow g_{7/2}$ neutron excitations are involved, beginning at excitation energies of 2184 keV and 1702 keV for positive- and negative-parity states, respectively. For the higher-spin states above the maximum angular momentum available from these active orbitals, breaking of the $Z = 38$ subshell occurs. Proton excitations $(\pi f_{5/2}/p_{3/2} \rightarrow g_{9/2})$ coupled with neutron $d_{5/2} \rightarrow g_{7/2}$ excitations result in γ transitions with energies greater than 2 MeV. Future experiments with higher statistics may help identify possible 2-MeV transitions associated with $N = 50$ core breaking, which are expected to be off-yrast. In the present work, no clear evidence for $N = 50$ core breaking is observed up to excitation energies of 9 MeV.

ACKNOWLEDGMENTS

The authors thank the accelerator staff at the Institute of Modern Physics for providing the stable beam.

References

[1] A. Bohr and B. R. Mottelson, *Nuclear Structure Volume Ⅱ: Nuclear Deformations* (Singapore: World Scientific, 1998).
[2] M. J. A. de Voigt, J. Dudek, and Z. Szymański, Rev. Mod. Phys. **55**, 949 (1983)
[3] A. Afanasjev, D. Fossan, G. Lane *et al.*, Phys. Rep. **322**, 1 (1999)
[4] S. S. Ghugre, B. Kharraja, U. Garg *et al.*, Phys. Rev. C **58**, 3243 (1998)
[5] B. Kharraja, S. S. Ghugre, U. Garg *et al.*, Phys. Rev. C **57**, 83 (1998)
[6] S. S. Ghugre, B. Kharraja, U. Garg *et al.*, Phys. Rev. C **61**, 024302 (1999)
[7] Y. H. Zhang, M. Hasegawa, W. T. Guo *et al.*, Phys. Rev. C **79**, 044316 (2009)
[8] Y. H. Wu, J. B. Lu, Z. Ren, *et al.*, Phys. Rev. C **105**, 034344 (2022)
[9] Z. G. Wang, M. L. Liu, Y. H. Zhang *et al.*, Phys. Rev. C **89**, 044308 (2014)
[10] D. Bucurescu, Z. Podolyák, C. Rusu *et al.*, Phys. Rev. C **71**, 034315 (2005)
[11] N. Fotiades, J. A. Cizewski, R. Krücken *et al.*, Eur. Phys. J. A **48**, 117 (2012)
[12] E. Cosman, D. Slater, R. F. Casten *et al.*, Phys. Rev. C **10**, 671 (1974)
[13] E. Flynn, O. Hansen, J. Sherman *et al.*, Nucl. Phys. A **264**, 253 (1976)
[14] W. L. Talbert, F. K. Wohn, L. J. Alquis *et al.*, Phys. Rev. C **23**, 1726 (1981)
[15] E. A. Stefanova, R. Schwengner, J. Reif *et al.*, Phys. Rev. C **62**, 054314 (2000)
[16] Y. Hao, Z. Ren, J.-B. Lu *et al.*, Phys. Rev. C **111**, 034312 (2025)
[17] Z. R. Jiang, Z. Q. Li, J. W. Sheng *et al.*, J. Phys. G **51**, 085102 (2024)
[18] S. F. Shen, K. M. Fang, J. H. Gu *et al.*, Eur. Phys. J. A **32**, 149 (2007)
[19] K. Krämer and B. Huber, Z. Physik **267**, 117 (1974)
[20] D. G. Sarantites and A. C. Xenoulis, Phys. Rev. C **10**, 2348 (1974)
[21] W. L. Zhan, J. W. Xia, H. W. Zhao *et al.*, Nucl. Phys. A **805**, 533c (2008)
[22] G. S. Li, X. H. Zhou, M. L. Liu *et al.*, Nucl. Instrum. Meth. A **1080**, 170804 (2025)
[23] F. Azaiez, Nucl. Phys. A **654**, 1003c (1999)
[24] D. G. Sarantites, Phys. Rev. C **12**, 1176 (1975)
[25] D. Hippe, B. Heits, H. W. Schuh *et al.*, Z. Phys. A **273**, 349 (1975)
[26] G. Winter, F. Dönau, L. Funke *et al.*, Nucl. Phys. A **291**, 401 (1977)
[27] W. B. C. K. A. Marshall, J. V. Thompson and M. W. Johns, Can. J. Phys. **56**, 117 (1978)
[28] W. Urban, K. Sieja, T. Rząca-Urban *et al.*, Phys. Rev. C **104**, 064309 (2021)
[29] N. Shimizu, T. Mizusaki, Y. Utsuno *et al.*, Comp. Phys. Comm. **244**, 372 (2019)
[30] M. Honma, T. Otsuka, T. Mizusaki *et al.*, Phys. Rev. C **80**, 064323 (2009)
[31] T. Otsuka, T. Suzuki, M. Honma *et al.*, Phys. Rev. Lett. **104**, 012501 (2010)
[32] T. Otsuka, R. Fujimoto, Y. Utsuno *et al.*, Phys. Rev. Lett. **87**, 082502 (2001)
[33] P. Federman and S. Pittel, Phys. Lett. B **69**, 385 (1977)
[34] P. Federman, S. Pittel, and A. Etchegoyen, Phys. Lett. B **140**, 269 (1984)
[35] Y. Wakabayashi, T. Fukuchi, Y. Gono *et al.*, J. Phys. Soc. Jpn. **76**, 114202 (2007)
[36] B. M. Preedom, E. Newman, and J. C. Hiebert, Phys. Rev. **166**, 1156 (1968)